



The influence of sludge ash and its active species on the combustion characteristics and kinetics of biomass: application of model-fitting method combined with master-plots method

Xingui Mo¹ · Jianqiang Ren¹ · Yaoyu Zhou¹ · Wenhan Jiang¹ · Jianbiao Chen¹ · Jinjiao Zhu² · Chao Wu³ · Yuezhao Zhu¹

Received: 27 February 2023 / Revised: 24 April 2023 / Accepted: 2 May 2023 / Published online: 8 May 2023
© The Author(s), under exclusive licence to Springer-Verlag GmbH Germany, part of Springer Nature 2023

Abstract

Combustion characteristics and kinetics of camellia seed shell (CS) with additions of sludge ash (SA) and its active species of CaO, Fe₂O₃, and SiO₂ were analyzed by thermogravimetry. The combustion paths of CS with the additives fell between “in situ combustion of carbon-containing components” and “complete volatiles release + char combustion.” In the view of heat release, the additions of SA active species increased the combustion performance of CS. A higher heating rate greatly increased the combustion performance, but the addition of CaO decreased the combustion performance. The combustion kinetic parameters of CS with the 10% additions of SA, CaO, Fe₂O₃, and SiO₂ were analyzed by combining Coats-Redfern and Malek methods. The distributions of the activation energies of the second combustion zone with certain additives were more centralized. It was found that the second combustion zones all followed $f(x) = (1 - x)^2$ at varied heating rates, while those of the third zone were not identical, and those of the fourth zone of CS + 10%CaO followed $f(x) = (1 - x)^{2/3}$.

Keywords Camellia seed shell · TGA–DSC analysis · Catalytic combustion Coats-Redfern method · Master-plots method

1 Introduction

Along with the global population boosting and economy developing, environment and energy have become the main problems of human concern [1, 2]. The rapid depletion of

fossil fuels and serious impacts on the environment during the application have attracted many attentions on the alternate energy sources in recent years [3, 4]. Among them, biomass energy has the superiorities of cleans and can be recycled for utilization [5–7]. Since the existing coal-fired boilers have been equipped with the perfect combustion system and flue gas purification equipment, biomass burned in the existing coal-fired facilities will be an important manner. It is the thermochemical reactions in the oxidative atmospheres by converting the chemical energy in the organic matters to generate heat, steam, and power [8, 9]. So, improving the biomass combustion efficiency and being suitable for the existing coal-fired boilers have been an important pursuit.

Recently, the production of various sludge also increases sharply with the progress of society, which has the properties of high moisture, perishable and stinky, and rich in the toxic and harmful substances that are difficult to be degraded. The incineration technology will realize the harmless, reduced, and resourceful disposal of sludge, which is very popular and practical. The incineration disposal can obtain a volume reduction for the sludge, while there are still a lot of sludge ash (SA), which has certain active species, such as CaO, Fe₂O₃, and SiO₂, and can play catalytic roles in the thermal

Highlights

- The effects of SA, CaO, Fe₂O₃, and SiO₂ on combustion of camellia seed shell were studied.
- Catalytic combustion performances were influenced by the additives and heating rates.
- Additions of SA active species were conducive to CS combustion in view of heat release.
- Catalytic combustion kinetics were gotten by Coats-Redfern combined with Malek method.

✉ Jianbiao Chen
jianbiaochen@njtech.edu.cn

- ¹ School of Energy Science and Engineering, Nanjing Tech University, Nanjing 211816, Jiangsu, China
- ² School of Automotive Engineering, Yancheng Institute of Technology, Yancheng 224051, Jiangsu, China
- ³ School of Applied Chemistry and Materials, Zhuhai College of Science and Technology, Zhuhai 519041, Guangdong, China

conversion of carbon-containing fuels. For example, Gao et al. [10, 11] used cost-effective catalyst of sludge ash in the pyrolysis of municipal solid waste (MSW), which not only confirmed the existence of active species, i.e., CaO, Fe₂O₃, and SiO₂, in a sludge ash, and also found that had certain catalytic roles in the thermal conversion of organic solid wastes. Nevertheless, the catalytic effects of sludge ash on the combustion of organic solid wastes have not been studied deeply yet, which motivated the implement of this work. In addition to this, the co-combustion strategy for the sludge disposal with biomass has been proposed by many researchers and engineers. Most of them mainly focused on the co-combustion behaviors, reaction kinetics, and gas emission, while played little attention on the potential catalytic roles of SA. For instance, Wu et al. [12], Huang et al. [13], and Hu et al. [14] studied the co-combustion of textile dyeing sludge with biomass, and found that the good combustion performance and pollutant emissions could be obtained by a proper selection of multiple wastes and operational conditions. So, to study the catalytic effects of SA and its active species in biomass, combustion is not only beneficial for studying the effect of mineral component on the co-combustion of sludge and biomass, but also help to realize the high-value utilization of SA in the process of the catalytic combustion of biomass.

The biomass combustion process is similar to that of other solid fuels, including the pyrolysis, volatile matters combustion, and char combustion [15, 16]. Up to now, many scholars are working to increase the formation of volatiles in combustion of various solid fuels, which is a vital manner to rise combustion performances of fuels [17–19]. A great number of studies have showed that the combustion of various fuels with appropriate catalysts, including alkali/alkaline earth metals [17], transition metals [20], rare earth metals [21], and so on, would be improved. It was due to that the additions of metal catalysts reduce the chemical-bond energy, decrease intermolecular forces, and rise the degradation of organic macromolecular and the condensation of products. Zhang et al. [22] used the thermogravimetric analyzer to study the catalytic effects of CeO₂, Fe₂O₃, and NiO on the combustion of bituminous coal, and found that the metal oxides would significantly enhance the transport of oxygen to the coal or chars surface and increase the combustion performances. Also, the apparent activation energies of coal combustion decreased with the presence of metal oxides. With regard to the biomass materials, the catalytic combustion characteristics were also studied to some extent. Cai et al. [23] carried out a kinetic analysis on the catalytic combustion of biomass after alkaline metals loaded pretreatment based on thermal analysis data. The kinetic parameters were analyzed by the integral Coats-Redfern method, and the most suitable kinetic functions

were pre-considered as the simple order reaction model $f(x) = (1 - x)^n$. It was observed that the activation energies of biomass combustion decreased after the alkaline metals loaded pretreatment.

To develop a low-cost catalyst from the solid wastes, the potential application of sludge ash, coal ash, and others was attempted in solid fuels combustion. As studied by Cheng et al. [24], the metal elements such as Na, Fe, Ca, and Al in the industrial wastes had certain catalytic effects on the coal combustion, which was revealed by the reduction of ignition temperature and increase of burnout efficiency. Song et al. [25] have reported the catalytic effects of CaO, Al₂O₃, Fe₂O₃, and red mud on *Pteris vittata* combustion through using thermogravimetric analysis, and observed that the presence of catalysts would change the emissions of gas products. The kinetic parameters were calculated by the Coats-Redfern method, and the best kinetic model was selected according to the linear regression coefficient R^2 . In the study of Hu et al. [26], the catalytic combustion kinetics of two bamboo residues with presence of sludge ash, CaO, and Fe₂O₃ were respectively analyzed by two iso-conversional methods, such as the Starink method and Tang method. The change trends of activation energy with conversion degree were revealed, but the kinetic model was not given.

According to the above reviewed literature, the present investigations contributed greatly to the catalytic effects of solid ash wastes and metal oxides on combustion characteristics and kinetic parameters of various solid fuels, but there also existed certain deficiencies, such as a lacking of catalytic analysis in the view of the exothermic values, and how to select the best kinetic function. The reviewed studies showed that the Coats-Redfern method seemed successfully in determining the catalytic combustion kinetic parameters, while for the possible reaction mechanism functions, their linear regression coefficients (R^2) were all very high, and thus it was hard to select the most suitable kinetic function [27, 28]. Thus, a further analysis on the catalytic combustion of biomass by the SA and its active species is necessary, especially, an insight into the determination of the kinetic parameters, since which is very vital to provide significant guidance on feasibility, design, and optimization of industrial combustion device.

The paper selected one typical SA and its active species such as CaO, Fe₂O₃, and SiO₂ as the additives to perform the catalytic combustion of biomass, a typical oil-plant waste, camellia seed shell (CS). The catalytic combustion experiments were carried out at distinct heating rates of 5, 10, 20, and 40 °C/min by using thermogravimetry (TGA) and differential scanning calorimetry (DSC). Hence, the main objectives of this work were: (1) Determining catalytic combustion reaction path by comparing with pyrolysis; (2) quantitatively analyzing the catalytic combustion performance of

CS from the perspective of TGA and DSC values; (3) applying the model-fitting and master-plots methods to calculate the catalytic combustion kinetic parameters.

2 Materials and methods

2.1 Materials preparation

Camellia oil is a unique woody edible oil in China with high unsaturated fatty acid content. In recent years, the state has encouraged camellia oil planting and vigorously developed the camellia oil industry. The data shows that China planted about 461.7 hectare of camellia oil in 2019, thus a great number of camellia seed shells (named as CS) can be used as biomass energy feedstock. So far, many researchers have used CS as a feedstock for the thermochemical conversion, such as the torrefaction [29], (co-)pyrolysis [30], and even catalytic co-pyrolysis [31], mainly based on its rich source, easy availability, and good fuel properties.

According to the standards of GB/T 28,731–2012 and 28,734–2012, the proximate and ultimate analysis of CS were separately studied by Vario Macro cube CHNS elemental analyzer (Elementar, Germany) and SDTGA5000 proximate analyzer (SUNDY enterprise Co., Ltd, Changsha, China). To ensure the reliability of the analytical results, all experiments were performed three times. The mean values and standard deviation were shown in Table 1. Similar to the most biomass materials, the volatile matters in the CS are high, and the ash content is low. The oxygen content in the CS is high to 44.69% (on dry basis), which is conducive to the thermal oxidative degradation reactions. The raw CS samples were first natural dried, then shredded to 80–100 mesh, dried at 105 °C until constant weight, and finally stored in a desiccator.

Moreover, the sludge ash (SA) prepared from sewage sludge in Wuxi city was selected as the additive for the CS combustion, which contained 39.28% CaO, 15.04% Fe₂O₃, and 17.85% SiO₂ according to XRF analysis. The above active species were also solely employed as the additive to reveal their respective action temperature range and degree. Fully mixed SA and its active species with the pre-treated CS powders via adequately mechanical vibrations, and the

weight proportions of SA were 10%, 20%, and 30%, and those of three active species were all kept at 10%. Finally, the prepared mixtures were stored in the desiccator for subsequent tests.

2.2 Experimental methods

The STA 449 F1 simultaneous thermal analyzer manufactured by NETZSCH, Germany was applied to analyze the thermal oxidative decomposition (or called combustion) process of CS with the presence of SA and its active species (CaO, Fe₂O₃, and SiO₂), as well as CS without additives. Prior to formal experiments, the stability and sensitivity of thermal analyzer were examined at one testing condition for three times. The experiments of thermal oxidative decomposition of CS with a presence of SA, CaO, Fe₂O₃, and SiO₂ were carried out from room temperature to 1000 °C. The heating rates were selected at 5, 10, 20, and 40 °C/min. The required oxidative environment was produced by the flow rate of 50 mL/min dried air. To reduce the mass and heat transfer influences, the initial weight of sample was constrained to a small and constant value of 6.0 ± 0.1 mg. To reveal the combustion reaction path of CS with a presence of SA, CaO, Fe₂O₃, and SiO₂, the CS samples were tested from room temperature to 1000 °C with a heating rate of 20 °C/min at a pure nitrogen atmosphere. For different conditions, the thermal analysis baselines were predetermined without a sample loading to reduce the influence of carrier gas buoyancy. All experiments repeated at least three times to ensure a reliable result.

2.3 Determination of catalytic combustion characteristic parameters

For better describing the catalytic effects of additives, such as SA, CaO, Fe₂O₃, and SiO₂ in this study, on the CS combustion, the characteristic parameters were determined from the TG and DTG curves during the catalytic combustion experiments, such as the ignition temperature T_i , °C; peak temperature T_p , °C; burnout temperature T_b , °C; the maximum weight loss rate $-R_p$, %/min; average weight loss rate $-R_v$, %/min; temperature range at half of $-R_p$ HTZ, °C; and the residual weight after combustion

Table 1 Proximate and ultimate analysis of camellia seed shell (CS)

Proximate analysis (wt%, ar ^a)				Ultimate analysis (wt%, db ^b)					LHV MJ/kg
M	VM	FC	A	C	H	O ^c	N	S	
6.56 ± 0.05	66.26 ± 0.09	24.51 ± 0.03	2.67 ± 0.13	45.67 ± 0.10	6.41 ± 0.03	44.69 ± 0.23	0.37 ± 0.008	0.19 ± 0.004	15.64 ± 0.18

^aAs received basis

^bDry basis

^cBy difference

W_r , %. According to the related literature, the combustion characteristic parameters can be determined by different methods, although there exist some slightly differences, the values can be in comparison as long as the definitions are consistent. The ignition temperature T_i was determined by the TG-DTG tangent approach as reported in the previous literature [16, 32]. The peak temperature T_p corresponded to the temperature point of DTG profile where the weight loss rate reached local maximum. The burnout temperature T_b was seen as the temperature point where the combustion reaction ceased.

The volatiles releasing, ignition, burnout, and comprehensive combustion performance of CS with the addition of SA, CaO, Fe₂O₃, and SiO₂ can be investigated by the complex indices, such as the devolatilization index D_i , %/min °C³; ignition index C_i , %/min³; burnout index C_b , %/min⁴; the comprehensive combustibility index CCI , %²/min²C³. The devolatilization index D_i is introduced to analyze the volatiles releasing performance in the combustion, which is defined as [23, 26]:

$$D_i = \frac{-R_{p2}}{T_v \times T_{p2} \times HTZ_2} \quad (1)$$

where $-R_{p2}$ and T_{p2} represent the maximum weight loss rate and corresponding temperature at the 2nd combustion zone. T_v is the initial devolatilization temperature. HTZ_2 refers to the temperature range where the weight loss rate was the half of $-R_{p2}$ at the 2nd combustion zone.

And, the ignition and burnout performances of CS with the presence of SA, CaO, Fe₂O₃, and SiO₂ during the combustion can be evaluated by the indices as [16]:

$$C_i = \frac{-R_p}{t_i \times t_p} \quad (2)$$

$$C_b = \frac{-R_p}{\Delta t_{1/2} \times t_p \times t_b} \quad (3)$$

where t_i , t_p , $\Delta t_{1/2}$, and t_b refer to the ignition time, peak time, time range at half of $-R_p$, and burnout time, respectively.

Moreover, the comprehensive combustibility index (CCI) is defined to evaluate the catalytic combustion of CS with the presence of SA, CaO, Fe₂O₃, and SiO₂ [23].

$$CCI = \frac{(-R_p) \times (-R_v)}{T_i^2 \times T_b} \quad (4)$$

where $-R_p$, $-R_v$, T_i , and T_b have the same definitions as above. As revealed by Eq. (4), the higher value of CCI is, the better combustion performance of the samples is.

2.4 Kinetics analysis method

2.4.1 Non-isothermal kinetics theory

The thermal oxidative decomposition of various solid fuels is a typical kind of heterogeneous solid-state reaction, which consists of complex chemical reactions and physical changes, and may be worked in several phases. However, the existing kinetic theory is based on the homogeneous and isothermal system, how does it apply to non-isothermal heterogeneous systems is a challenge. Changing the concentration c in a homogeneous system into conversion degree x , and dividing the non-isothermal process into innumerable isothermal steps are a generally accepted practice.

$$x_i = \frac{w_{i0} - w_{it}}{w_{i0} - w_{i\infty}} \quad \text{for zone } i \quad (5)$$

where w_{i0} , and $w_{i\infty}$ represent sample weights at the beginning and the end of the zone i during the thermal oxidative decomposition reaction, respectively. w_{it} is the instantaneous sample weight at time t of the zone i . x_i is the conversion degree of the zone i [33–35]. Moreover, on the basis of full reference to the relevant literature [36, 37], to ensure the high accuracy of kinetics analysis results, the x values applied in calculation were in a wide range of 0.05–0.95 with the small step of 0.01.

Then, each combustion zone is described by a reaction rate equation.

$$\frac{dx_i}{dt} = k(T_i)f(x_i) = A_i \exp\left(-\frac{E_i}{RT_i}\right)f(x_i) \quad (6)$$

where dx_i/dt is the conversion reaction rate. $k(T_i)$ is the reaction constant that is expressed by the Arrhenius law. A_i , E_i , R , and T_i in the Arrhenius equation are the pre-exponential factor, activation energy, gas constant, and absolute reaction temperature, respectively. $f(x_i)$ is the differential kinetic mechanism function.

For the combustion of CS with the presence of additives at non-isothermal conditions, the tests were carried out at the special heating rate of $\beta = dT/dt$. Equation (6) can be rewritten as [38]:

$$\beta \frac{dx_i}{dT} = A_i \exp\left(-\frac{E_i}{RT_i}\right)f(x_i) \quad (7)$$

Equation (7) is the general kinetic equation for a TG curve obtained at a constant heating rate, and also the basic equation for the differential kinetic analysis.

Performing the integral for the both sides of Eq. (7), which can be further transferred into:

$$\int_0^{x_i} \frac{dx_i}{f(x_i)} = g(x_i) = \frac{A_i}{\beta} \int_{T_0}^T \exp\left(-\frac{E_i}{RT_i}\right) dT = \frac{A_i}{\beta} p(u_i) \quad (8)$$

where $u_i = E_i/RT_i$, $p(u_i)$ in Eq. (8) is the temperature integral, which has no exact analytical solution, and usually estimated by various empirical interpolation formulas.

According to the reviewed literature, it is found that the integral Coats-Redfern method were popular in the determination of kinetic parameters, such as E , A , and $f(x)$. The series expansion of $p(u_i)$ in Coats-Redfern method is:

$$p(x_i) = \frac{e^x}{x^2} \left(1 + \frac{2!}{x} + \frac{3!}{x^2} + \dots\right) \quad (9)$$

Adopting the first three terms of Eq. (9), substituting it into Eq. (8) and separating variables, and taking a logarithm on both sides, the equation of Coats-Redfern method is gotten as:

$$\ln \frac{g(x_i)}{T_i^2} = \ln \frac{A_i R}{\beta E_i} \left(1 - \frac{2RT_i}{E_i}\right) - \frac{E_i}{RT_i} \quad (10)$$

For the general temperature range and most E values, the value of E/RT is much larger than 1, thus Eq. (10) can be simplified as:

$$\ln \frac{g(x_i)}{T_i^2} = \ln \frac{A_i R}{\beta E_i} - \frac{E_i}{RT_i} \quad (11)$$

The solid-state reaction can be described by various forms of $g(x)$, which have been presented in Table 2. Inserting the correct $g(x_i)$ into Eq. (11), the plot of $\ln g(x_i)/T_i^2$ versus $1/T_i$ is the straight line, whose slope and intercept are $-E_i/R$ and $\ln A_i R/\beta E_i$, respectively. Then, the activation energy E_i and pre-exponential factor A_i can be determined [39, 40].

2.4.2 Kinetic function screened by Malek method

In Coats-Redfern method, the estimation of E , A , and $f(x)$ mainly relied on the good linearity. However, a good linearity cannot guarantee the kinetic function selected is reasonable. So, being combined with other methods to screen the correct kinetic function is very necessary, one of the most common is the master-plots method, including the forms of differential, integral, and their combination [41]. Among them, the Malek method is one of the master-plots methods, which can be used to determine the kinetic mechanism function by introducing the equation of $y(x)$ [42].

$$y(x) = \left(\frac{T}{T_{0.5}}\right)^2 \frac{dx/dt}{(dx/dt)_{0.5}} = \frac{f(x)g(x)}{f(0.5)g(0.5)} \quad (12)$$

where $y(x)$ is the self-definition function. dx/dt , $f(x)$, and $g(x)$ have the same definitions as above.

In Eq. (12), the plots of $\left(\frac{T}{T_{0.5}}\right)^2 \frac{dx/dt}{(dx/dt)_{0.5}}$ and $\frac{f(x)g(x)}{f(0.5)g(0.5)}$ versus x are respectively the experimental and theoretical master plots, which are respectively based on the experimental data and standard mechanism function. Therefore, it can be seen that the Malek method is a relatively objective approach, when the best kinetic function is selected, the experimental plots on the left of Eq. (12) will overlap the theoretical plots on the right of Eq. (12) for the given x .

3 Results and discussion

3.1 Catalytic pyrolysis and combustion process

To confirm the combustion reaction paths of CS with additions of SA and its active species of CaO, Fe₂O₃, and SiO₂, TG and DTG curves from the pyrolysis and combustion at the heating rate of 20 °C/min were compared together, as shown in Fig. 1.

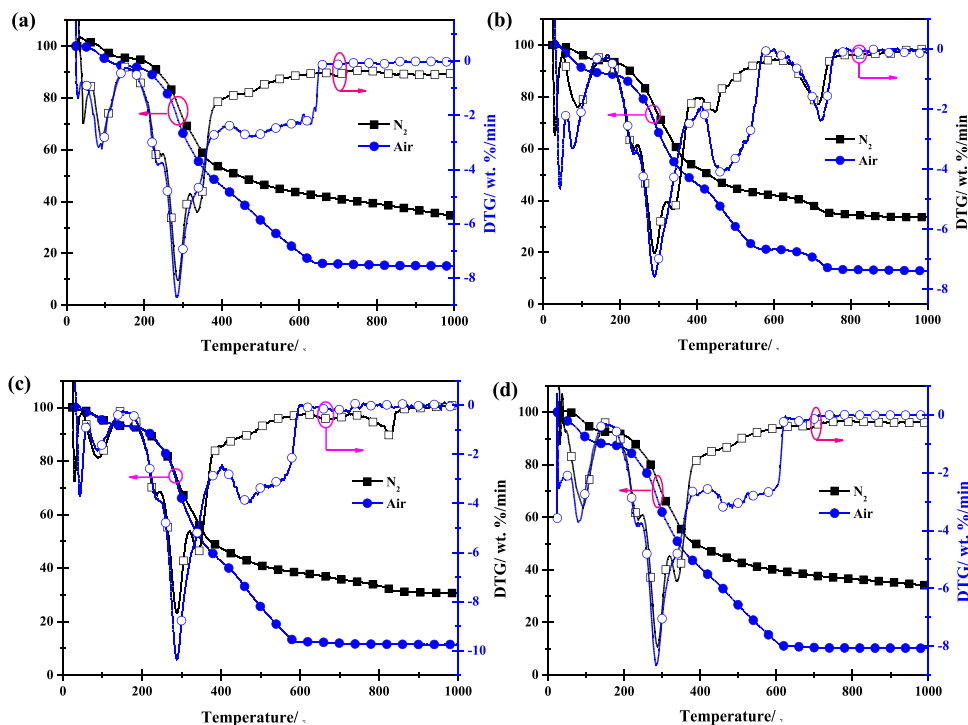
As shown in Fig. 1a, the pyrolysis of CS with 10% SA addition mainly included two weight loss zones of moisture release and devolatilization, while the combustion process of that had three weight loss zones, such as the moisture release, devolatilization and gas phase combustion, and the oxidation of chars. It was observed that the TG curve of the CS combustion with 10% SA addition was invariably lower than that of the pyrolysis at the whole heating process. A close attention was paid on the first two zones, where the weight loss for the combustion was slightly larger than that of the pyrolysis. It was because though the oxygen existed in the reaction atmosphere, the reaction temperature was at relatively low value, the weight loss of the combustion was ascribed to release of volatiles, and the oxygen would react with the volatile matters and then slightly increase weight loss. Also, as seen from the DTG data in Fig. 1(a), the value from the combustion was higher than that from the pyrolysis. So, the combustion path of CS with 10%SA addition fell between “in situ combustion of carbon-containing components” and “complete volatiles release + char combustion” [43]. Similar findings were also found in the catalytic pyrolysis/combustion of CS with addition of 10%CaO and 10%SiO₂, their TG and DTG curves were separately shown in Fig. 1b and d. But, the differences in TG curves between the combustion and pyrolysis of CS with 10%Fe₂O₃ started at the 2nd peak temperature rather than the beginning of heating, seen in Fig. 1c).

Further, it is found that the differences between the DTG curves of combustion and pyrolysis of CS with 10%CaO and 10%Fe₂O₃ at their 2nd zones were more obvious than those with addition of 10%SA and 10%SiO₂. The main reason was due to that the CaO and Fe₂O₃ played roles of CO₂ adsorbent and lattice oxygen supplier, respectively, which

Table 2 Most frequently used kinetic model and its corresponding mechanism of solid state process

No	Symbol	Name of functions	$g(x)$	$f(x)$	Rate-determining mechanism
Chemical process or mechanism non-invoking equations					
1	$F_{1/3}$	One-third order	$3/2[1-(1-x)^{2/3}]$	$(1-x)^{1/3}$	Chemical reaction
2	$F_{3/4}$	Three-quarters order	$4[1-(1-x)^{1/4}]$	$(1-x)^{3/4}$	Chemical reaction
3	$F_{3/2}$	One and a half order	$2[(1-x)^{-1/2}-1]$	$(1-x)^{3/2}$	Chemical reaction
4	F_2	Second order	$(1-x)^{-1}-1$	$(1-x)^2$	Chemical reaction
5	F_3	Third order	$[(1-x)^{-2}-1]/2$	$(1-x)^3$	Chemical reaction
Acceleratory rate equations					
6	$P_{3/2}$	Mampel power law	$x^{3/2}$	$(2/3)x^{-1/2}$	Nucleation
7	$P_{1/2}$	Mampel power law	$x^{1/2}$	$2x^{1/2}$	Nucleation
8	$P_{1/3}$	Mampel power law	$x^{1/3}$	$3x^{2/3}$	Nucleation
Sigmoidal rate equations or random nucleation and subsequent growth					
9	A_1, F_1	Avrami–Erofeev equation	$-\ln(1-x)$	$1-x$	Assumed random nucleation and its subsequent growth, $n=1$
10	$A_{3/2}$	Avrami–Erofeev equation	$[-\ln(1-x)]^{2/3}$	$1.5(1-x)[-\ln(1-x)]^{1/3}$	Assumed random nucleation and its subsequent growth, $n=1.5$
11	A_2	Avrami–Erofeev equation	$[-\ln(1-x)]^{1/2}$	$2(1-x)[-\ln(1-x)]^{1/2}$	Assumed random nucleation and its subsequent growth, $n=2$
12	A_3	Avrami–Erofeev equation	$[-\ln(1-x)]^{1/3}$	$3(1-x)[-\ln(1-x)]^{2/3}$	Assumed random nucleation and its subsequent growth, $n=3$
13	A_4	Avrami–Erofeev equation	$[-\ln(1-x)]^{1/4}$	$4(1-x)[-\ln(1-x)]^{3/4}$	Assumed random nucleation and its subsequent growth, $n=4$
Deceleratory rate equations					
Phase boundary reaction					
14	R_1, F_0, P_1	Power law	x	1	Contracting disk
15	$R_2, F_{1/2}$	Power law	$1-(1-x)^{1/2}$	$2(1-x)^{1/2}$	Contracting cylinder (cylindrical symmetry)
16	$R_3, F_{2/3}$	Power law	$1-(1-x)^{1/3}$	$3(1-x)^{2/3}$	Contracting sphere (spherical symmetry)
Based on the diffusion mechanism					
17	D_1	Parabola low	x^2	$1/2x$	One-dimensional diffusion
18	D_2	Valensi equation	$(1-x)\ln(1-x)+x$	$[-\ln(1-x)]^{-1}$	Two-dimension diffusion
19	D_3	Jander equation	$[1-(1-x)^{1/3}]^2$	$1.5(1-x)^{2/3}[1-(1-x)^{1/3}]^{-1}$	Three-dimensional diffusion, spherical symmetry
20	D_4	Ginstling–Brounstein equation	$(1-2x/3)-(1-x)^{2/3}$	$1.5[(1-x)^{-1/3}-1]^{-1}$	Three-dimensional diffusion, cylindrical symmetry
21	D_5	Zhuravlev, Lesokin, Tempelman equation	$[(1-x)^{-1/3}-1]^2$	$1.5(1-x)^{4/3}[(1-x)^{-1/3}-1]^{-1}$	Three-dimensional diffusion
22	D_6	Anti-Jander equation	$[(1+x)^{1/3}-1]^2$	$1.5(1+x)^{2/3}[(1+x)^{1/3}-1]^{-1}$	Three-dimensional diffusion
23	D_7	Anti-Ginstling-Brounstein equation	$1+2x/3-(1+x)^{2/3}$	$1.5[(1+x)^{-1/3}-1]^{-1}$	Three-dimensional diffusion
24	D_8	Anti-Zhuravlev, Lesokin, Tempelman equation	$[(1+x)^{-1/3}-1]^2$	$1.5(1+x)^{4/3}[(1+x)^{-1/3}-1]^{-1}$	Three-dimensional diffusion
Another kinetics equations with unjustified mechanism					
25	G_1		$1-(1-x)^2$	$1/2(1-x)$	
26	G_4		$[-\ln(1-x)]^2$	$1/2(1-x)[-\ln(1-x)]^{-1}$	
27	G_5		$[-\ln(1-x)]^3$	$1/3(1-x)^2[-\ln(1-x)]^{-2}$	
28	G_6		$[-\ln(1-x)]^4$	$1/4(1-x)^3[-\ln(1-x)]^{-3}$	
29	G_7		$[1-(1-x)^{1/2}]^{1/2}$	$4\{(1-x)[1-(1-x)^{1/2}]\}^{1/2}$	
30	G_8		$[1-(1-x)^{1/3}]^{1/2}$	$6\{(1-x)^{2/3}[1-(1-x)^{1/3}]\}^{1/2}$	

Fig. 1 TG-DTG curves of pyrolysis and combustion of **a** CS + 10% SA, **b** CS + 10% CaO, **c** CS + 10% Fe₂O₃, **d** CS + 10% SiO₂ at 20 °C/min



had promoted the occurrence of related reactions. With the reaction temperature increasing, one more weight loss peak would be found at a high temperature for the pyrolysis and combustion of CS with 10%CaO, which was mainly due to in-situ adsorption of CO₂ by CaO to form CaCO₃ at low temperature, and then be decomposed at the high temperature. As for Fig. 1c, for the pyrolysis of CS with 10%Fe₂O₃, one more weight loss peak also appeared at a high temperature. It was due to the reduction reactions between metal oxides and chars, such as $2\text{Fe}_2\text{O}_3 + 3\text{C} \rightarrow 4\text{Fe} + 3\text{CO}_2$ $\Delta H_{650^\circ\text{C}} = 431.6$ kJ/mol and $\text{Fe}_3\text{O}_4 + 2\text{C} \rightarrow 3\text{Fe} + 2\text{CO}_2$ $\Delta H_{650^\circ\text{C}} = 296.8$ kJ/mol.

3.2 Combustion of CS with different SA additions

The TG and DTG curves of CS combustion with different SA additions were presented in Fig. 2. As can be seen from Fig. 2a, the TG curve shapes of the CS combustion changed slightly with blending diverse SA proportions. As expected, with the SA addition increasing, the retention ratios of the solid products increased, which was ascribed to the thermal stability of SA components. The residues after the CS combustion with additions of 0, 10%, 20%, and 30%SA were 2.47%, 14.76%, 22.27%, and 31.47%, respectively. The terminal temperatures of varied samples were 619.6, 649.2, 659.2, and 649.0 °C, respectively, showing a trend of first increase and then decrease. The similar change trends were also found in the peak temperatures of 2nd zone shown in Fig. 2b. The delay of characteristic temperature could be

due to the close physical contact between CS and SA, which changed the void spaces of CS, and then affected the sensitivity of the combustion reaction.

The theoretical TG and DTG curves assuming no reaction between CS and SA were obtained and shown as dash dot lines in Fig. 2. The weight loss values from the experiments were less than the calculated ones with different SA additions, corresponding experimental weight loss rates were also smaller. As seen from Fig. 2a, the difference between the experimental and calculated values decreased with the SA addition ratio. Though the SA was rich in Fe₂O₃, which could supply lattice oxygen [O] during the CS combustion and promote the conversion of carbon materials, the oxygen in the air will quickly add into the SA.

3.3 Catalytic combustion process analysis

To analyze the catalytic effects of SA and its active species on CS combustion characteristics, the TG and DTG curves of the CS combustion with 10% additions of SA, CaO, Fe₂O₃, and SiO₂ at diverse heating rates of 5, 10, 20, and 40 °C/min were studied. For the combustion of CS + 10% SA, shown in Fig. 3(a1–2), as the heating rate went from 5 to 40 °C/min, the TG and DTG curves both shifted to the high temperature. This is thermal hysteresis, and common for varied non-isothermal tests [44, 45]. According to the DTG curve in Fig. 3b, the combustion of CS + 10% SA had the moisture release below 135.2–175.6 °C (depending on β_s), volatile matters release in the middle temperature

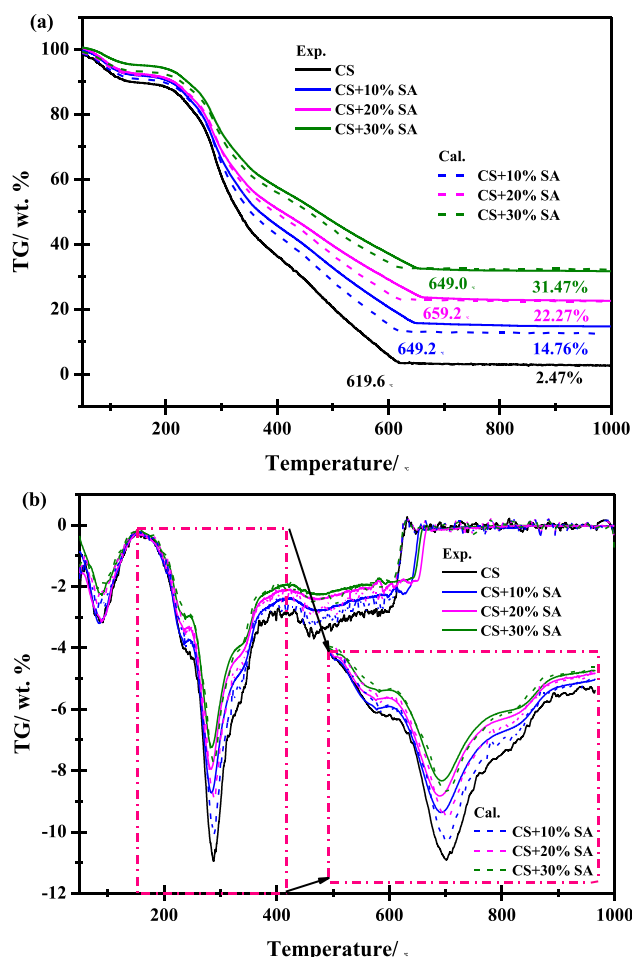


Fig. 2 a TG and b DTG curves of the combustion of CS with different SA additions

range, and chars combustion beyond 380.0–415.2°C (depending on β s). In addition, it was found that the patterns of thermal curves of the first two zones were almost not changed with β increasing, but those of the third zone changed evidently.

With the additions of Fe_2O_3 and SiO_2 , as shown in Fig. 3(c1-2) and (d1-2), the combustion of CS was also roughly divided into three zones. The devolatilization temperature of CS + 10% Fe_2O_3 ranged from 130.6–175.7°C to 385.0–433.2°C (depending on β s), and that of CS + 10% SiO_2 ranged from 140.3–170.7°C to 402.8–438.4°C (depending on β s). Hence, on the view of devolatilization temperature, the additions of Fe_2O_3 and SiO_2 had a slight effect on the combustion of CS. For the combustion of CS + 10% CaO, as shown in Fig. 3(b1-2), the process contained four zones, such as moisture release, devolatilization, char combustion, and thermal decomposition of carbonate. The initial decomposition temperature of the carbonate from the CS + 10% CaO combustion were 555.2, 570.5, 590.2, and 715.2 °C at 5, 10, 20, and 40 °C/min, respectively.

The thermal evolution of the combustion of CS with additions of SA, CaO, Fe_2O_3 , and SiO_2 at heating rates of 5, 10, 20, and 40 °C/min were studied by DSC technology. As shown in Fig. 3, the DSC shapes were roughly similar, but differences existed in peak heights and breadths. It was found that the peak position and number in the DSC curve corresponded to those in the DTG. The thermal events for the first zone were all endothermic, while those for the second and third zones were exothermic, corresponded to the related reactions referred above. An additional endothermic peak in the DSC of CS + 10% CaO combustion was found at the high temperature, which was due to the decomposition of carbonate ($\text{CaCO}_3 \rightarrow \text{CaO} + \text{CO}_2$ $\Delta H_{650^\circ\text{C}} = 170.5$ kJ/mol) that pre-formed by the reactions, such as $\text{CaO} + \text{CO}_2 \rightarrow \text{CaCO}_3$ $\Delta H_{650^\circ\text{C}} = -170.5$ kJ/mol, $\text{CaO} + \text{H}_2\text{O} \rightarrow \text{Ca(OH)}_2$ $\Delta H_{650^\circ\text{C}} = -93.0$ kJ/mol, and $\text{Ca(OH)}_2 + \text{CO}_2 \rightarrow \text{CaCO}_3 + \text{H}_2\text{O}$ $\Delta H_{650^\circ\text{C}} = -77.5$ kJ/mol. The DSC is a function of temperature, which can be written as $h(T)$. Further, the exothermic value of CS combustion with additions of SA and its active species can be calculated by the integral of DSC curve.

$$Q_{T_1 \rightarrow T_2} = \lambda \int_{T_1}^{T_2} h(T) dT \quad (13)$$

where $Q_{T_1 \rightarrow T_2}$ is the exothermic value; λ is the thermal analyzer constant; $h(T)$ is the heat flow.

As shown in Fig. 3(a3-d3), the shaded area between DSC curve and baseline was exothermic value of the sample combustion. It was found that, no matter for CS with SA or its active species, the shaded area for the char combustion was larger than that of the combustion of volatiles at any heating rate, meaning that the exothermic value of sample was dominant by the char combustion. The similar DSC curves were also found in the combustion of *Pteris vittata* as reported by Song et al. [46] that there were two different peaks during programmed heating process, corresponded to the volatiles combustion and chars combustion, respectively. As reported by Li et al. [45], during the combustion of camphor biomass waste, the DSC curve was also divided into two stages, while in the combustion bituminous coal, the DSC curve just had one prominent exothermic peak [22].

3.4 Catalytic combustion characteristic parameters

Catalytic combustion characteristic parameters of CS with 10% additions of SA, CaO, Fe_2O_3 , and SiO_2 were determined from TG and DTG curves, and the results were listed in Table 3. Since the weight loss of zone I was caused by the moisture release, the contributions on the combustion process could be neglected, thus its characteristic parameters were not analyzed. As given in Table 3, whether CS blended with SA or its active species, with the β value increasing, the

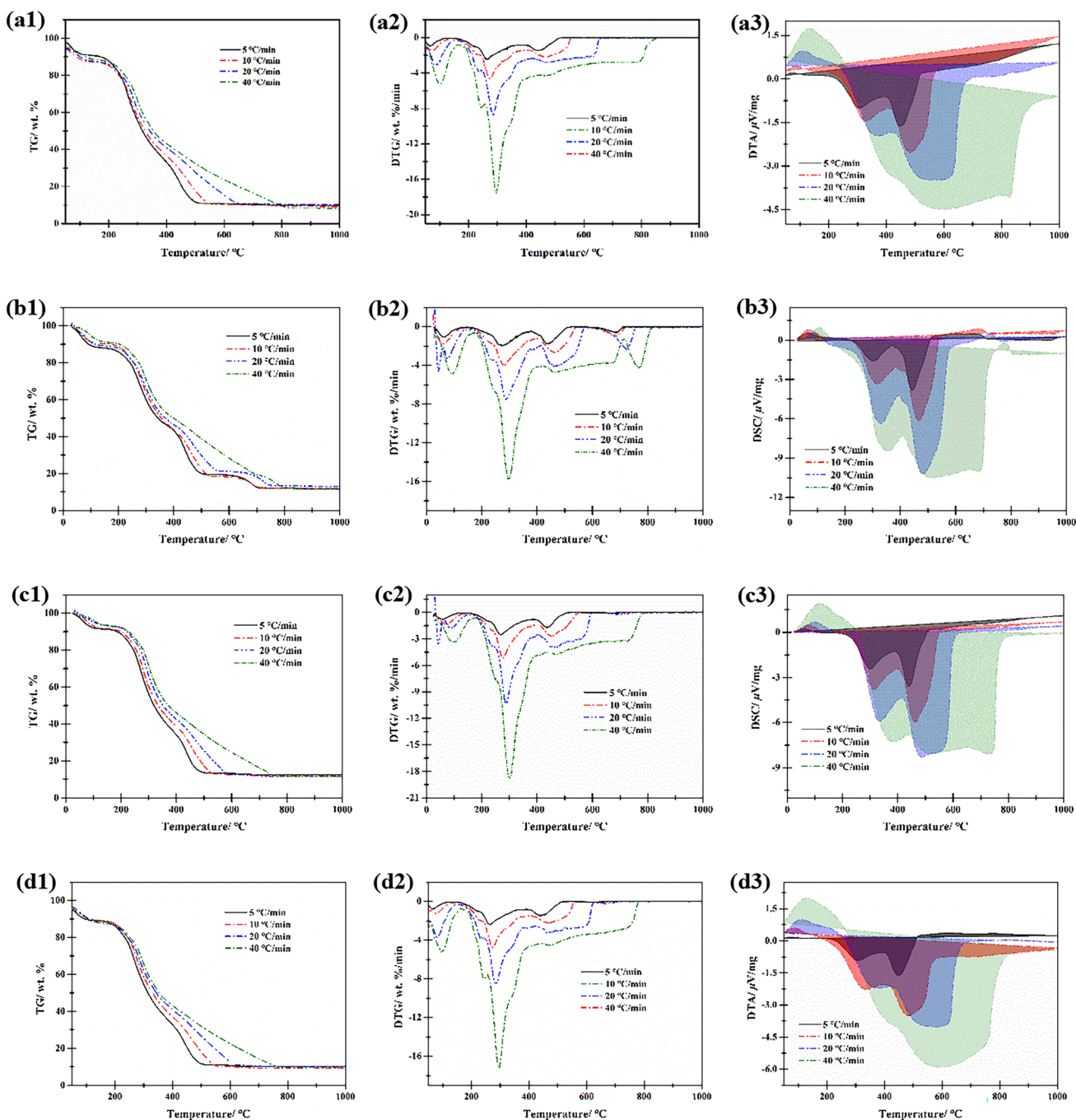


Fig. 3 TG, DTG, and DSC curves of CS with SA and its active species at varied heating rates. (a1-3) CS+10%SA, (b1-3) CS+10%CaO, (c1-3) CS+10%Fe₂O₃, (d1-3) CS+10%SiO₂

characteristic temperatures, such as T_i , T_{p2} , T_{p3} , T_{p4} , and T_b , all shifted toward the higher temperature. As for the characteristic weight loss rates, such as $-R_{p2}$, $-R_{p2}$, $-R_{p2}$, and $-R_v$, when the β value went from 5 to 40 °C/min, the values clearly increased. The $-R_v$ values for the CS combustion with SA were 1.16, 2.05, 3.38, and 4.88%/min at 5, 10, 20, and 40 °C/min, respectively. As for the values of HTZ , the variation trends with the β value were different at different

weight loss zones. At zone 2, the HTZ_2 values of varied samples were irregularly with β increasing, but the HTZ_3 and HTZ_4 monotonically increased. Further, the combustion performance indices were studied, and the results were listed in Table 4. It was found that, no matter CS blended with SA or its active species, the residual weights after combustion (W_r) were almost not affected by the β variation. As the β increased, the D_i values of all samples grew up,

Table 3 Characteristic parameters of CS combustion with 10% addition of SA, CaO, Fe₂O₃, and SiO₂

Samples	β °C/min	T_i °C	Zone 2			Zone 3			Zone 4			$-R_v$ %/min	T_b °C
			T_{p2} °C	$-R_{p2}$ %/min	HTZ_2 °C	T_{p3} °C	$-R_{p3}$ %/min	HTZ_3 °C	T_{p4} °C	$-R_{p4}$ %/min	HTZ_4 °C		
CS + SA	5	224.2	263.2	2.40	55.7	446.0	1.48	71.3				1.16	518.4
	10	231.9	275.2	4.55	59.3	472.2	2.20	136.7				2.05	556.7
	20	239.5	285.2	8.67	60.7	486.3	2.78	317.1				3.38	653.2
	40	247.0	295.4	17.70	57.5	480.2	4.22	639.6				4.88	846.0
CS + CaO	5	219.2	277.5	1.91	79.0	440.0	1.77	77.1	686.1	0.59	31.3	0.66	721.7
	10	224.3	280.2	3.97	68.5	462.8	2.68	105.0	688.6	0.99	35.1	1.66	724.2
	20	239.5	290.3	7.58	71.1	462.8	4.12	169.4	724.2	2.33	39.5	2.98	762.2
	40	252.2	297.8	15.85	66.5	467.9	4.77	455.5	769.8	4.32	45.2	4.86	818.1
CS + Fe ₂ O ₃	5	234.4	267.4	2.54	54.0	440.0	1.68	53.8				1.02	516.2
	10	236.9	277.5	5.14	54.5	452.6	2.68	123.7				2.59	554.2
	20	244.6	290.3	10.27	56.5	470.4	3.90	221.1				4.83	597.3
	40	257.2	303.0	18.75	66.4	475.6	4.69	549.1				5.33	785.2
CS + SiO ₂	5	219.2	263.2	2.43	52.1	447.6	1.46	69.1				1.02	520.4
	10	232.2	277.2	4.82	54.8	469.4	2.20	145.9				2.54	558.6
	20	236.9	285.2	8.46	47.2	470.4	4.46	273.6				4.34	627.0
	40	244.6	297.3	17.20	55.0	483.0	5.33	531.2				5.27	777.8

indicating that a higher β value led to more concentrated combustion zone and better burnout performance. Similarly, for all samples, the indices of C_i , C_b , and CCI increased significantly with the β increasing, indicating that the better ignition, burnout, and comprehensive performance would be obtained at the higher β value. Compared the indices of D_i , C_i , C_b , and CCI between varied samples, it was observed

that the values of CS + 10%SA were higher than those of CS + 10%CaO at the same β , but lower than those of CS with 10% additions of Fe₂O₃ and SiO₂. In the research of Song et al. [25], the similar phenomena were also reported on catalytic effects of red mud, CaO, Al₂O₃, and Fe₂O₃ on *Pteris vittata* combustion. Fang et al. [47, 48] have studied the effects of additives on thermal decomposition of paper

Table 4 Catalytic combustion performance indices of CS with 10% addition of SA, CaO, Fe₂O₃, and SiO₂

Samples	β °C/min	T_v °C	t_i min	t_p min	t_b min	$\Delta t_{1/2}$ min	W_r %	$10^6 \times D_v$ %/(min·°C ³)	C_i %/min ³	$10^4 \times C_b$ %/min ⁴	$10^7 \times CCI$ % ² /(min ² ·°C ³)
CS + SA	5	142.0	44.84	52.64	103.68	11.14	11.12	1.15	1.02	0.39	1.07
	10	142.0	23.19	27.52	55.67	5.93	9.15	1.96	7.13	5.01	3.12
	20	154.6	11.98	14.26	32.66	3.04	14.76	3.24	50.77	61.32	7.83
	40	162.8	6.18	7.39	21.15	1.44	8.62	6.40	388.14	788.55	16.73
CS + CaO	5	145.8	43.84	55.50	144.34	15.81	11.54	0.60	0.79	0.15	0.36
	10	246.0	22.43	28.02	72.42	6.85	11.56	0.84	6.32	2.86	1.81
	20	254.8	11.98	14.52	38.11	3.55	12.84	1.44	43.61	38.56	5.17
	40	170.0	6.31	7.45	20.45	1.66	11.97	4.71	337.66	625.89	14.80
CS + Fe ₂ O ₃	5	130.6	46.88	53.48	103.24	10.81	12.35	1.35	1.01	0.43	0.91
	10	250.2	23.69	27.75	55.42	5.45	11.90	1.36	7.82	6.13	4.28
	20	262.0	12.23	14.52	29.87	2.83	11.50	2.39	57.85	83.85	13.87
	40	175.7	6.43	7.58	19.63	1.66	11.51	5.31	384.95	760.10	19.25
CS + SiO ₂	5	140.3	43.84	52.64	104.08	10.42	11.57	1.26	1.05	0.43	0.99
	10	249.8	23.22	27.72	55.86	5.48	11.63	1.27	7.49	5.68	4.06
	20	261.6	11.85	14.26	31.35	2.36	11.91	2.40	50.09	80.17	10.44
	40	170.7	6.12	7.43	19.45	1.37	11.69	6.17	378.44	866.05	19.48

sludge and municipal solid waste by TGA, which were MgO, Al₂O₃, ZnO, and activated carbon. The results showed that the comprehensive performance indices were also affected by the additives, and their values became lower than those of samples without additives.

3.5 Catalytic combustion kinetics analysis

3.5.1 Evaluation on activation energy

According to the reviewed literature, it is found that the integral Coats-Redfern approach was widely used in the kinetic parameters calculation of the catalytic combustion of various solid fuels, and a series of relatively good results were obtained. Thus, the catalytic combustion kinetics of CS were also analyzed by integral Coats-Redfern approach in this paper. According to the 30 common used kinetic functions $g(x)$ that given in Table 2, inserting them into the Coats-Redfern equation of Eq. (11), the apparent activation energy (E) of different combustion zones could be estimated from the experimental data at four diverse heating rates of 5, 10, 20, and 40 °C/min, and the results were shown in Fig. 4, also including their regression coefficients (R^2).

As presented in Fig. 4a, with the β value went from 5 to 40 °C/min, the E values of the zone 2 of the CS + 10%SA combustion were almost not affected, but those of the zone 3 strictly reduced monotonically. For the listed 30 kinds of $g(x)$ functions, the E values of the zone 2 ranged from 3.0 to 215.0 kJ/mol, but those of the zone 3 distributed in a wide range from 30.0 to 525.0 kJ/mol, and the E values of the zone 3 were larger than those of the zone 2 at the identical $g(x)$. Observed from Fig. 4b, for the most $g(x)$, the R^2 data were all close to 1.0, and the R^2 data of zone 2 were higher than those of zone 3. It was because the relatively singular reactions occurred in the zone 2 where the volatiles released, while the gas–solid and solid–solid reactions between air and pyrolytic char, additive and char, occurred in the zone 3, where the oxygen absorption, oxidations, and products desorption continuously occurred.

Seen in Fig. 4e and g, the effects of heating rates (β s) on the E values of the combustion of CS with the 10% additions of Fe₂O₃ and SiO₂, were similar to those of CS + 10% SA. However, for 30 kinds of $g(x)$ functions, the E values distributions of two catalytic combustion zones were quite different from those of CS + 10%SA. The E values of zone 2 of CS + 10% Fe₂O₃ combustion ranged from 10.0 to 240.0 kJ/mol, and the most of them fell into the range of 10.0–160.0 kJ/mol, but the E values of zone 3 fell into 30.0–400.0 kJ/mol, and decreased with the β value increasing. As for the combustion of CS + 10%SiO₂, the E values of the zone 2 fell into 5.0–225.0 kJ/mol, while those of the zone 3 ranged from 40.0 to 400.0 kJ/mol. It could be observed from Fig. 4(g) that the E values of the two combustion zones

of CS + 10%SiO₂ almost fell below 240.0 kJ/mol. With regard to the catalytic combustion of CS with 10%CaO addition, with the β value increasing, the E values of the zone 2 almost kept constant, but those of the zone 3 reduced, and the zone 4 showed an increasing trend. As shown in Fig. 4(d), for the 30 kinds of $g(x)$, the R^2 data from the zone 4 of CS + 10% CaO combustion were the highest, and those of the zone 2 took the second place, and the zone 3 had the minimum. It was because the relatively single reactions occurred in the zone 4, such as CaCO₃ → CaO + CO₂, and some simple volatiles release reactions occurred in the zone 2, but the complicated oxidation reactions between char and oxygen/CaO took place in the zone 3.

3.5.2 Kinetic mechanism function screening

Based on the kinetics of CS catalytic combustion by the integral Coats-Redfern method, it is found that the most of $g(x)$ kinetic models applied all showed good linearity. Thus, the best kinetic functions of various combustion zones of CS with 10% addition of SA CaO, Fe₂O₃, and SiO₂ were hard to be determined just on basis of the data of R^2 . Thus, to screen the most appropriate kinetic model by combining the master-plots method, such as the Malek equation, was very necessary.

According to Eq. (12), the experimental plots of varied combustion zones of CS blended with 10% SA and CaO, Fe₂O₃, and SiO₂ were obtained by the data at different heating rates of 5, 10, 20, and 40 °C/min, and then compared with the theoretical plots that obtained by 30 kinds of standard mechanism functions listed in Table 2, and the results were shown in Fig. 5. For the zone 2 of CS combustion with 10% additions of SA, CaO, Fe₂O₃, and SiO₂, respectively shown in Fig. 5a, c, f, and h, the experimental $y(x)$ obtained at different heating rates were almost overlapped with each other, and presented a good agreement with the standard curve of No. 4, and the mechanism was the second order reaction $f(x) = (1 - x)^2$. As shown in Fig. 5b, d, g, and i, the experimental $y(x)$ of the zone 3 obtained at different heating rates deviated with each other, and corresponded to distinct kinetic mechanisms. The gas–solid and solid–solid reactions in the zone 3 at 5 °C/min were in a good agreement with the standard curve of No. 3, but those at 10 and 20 °C/min were close to the standard curve of No. 19, and that at 40 °C/min was hard to find one standard curve that really fitted the experimental $y(x)$. So, the kinetic mechanism of the third combustion zone at 40 °C/min should went back to combine with R^2 value to make a comprehensive decision. With regard to the zone 4 of CS + 10%CaO combustion, the experimental $y(x)$ obtained at different heating rates were almost overlapped with each other, and showed a good agreement with the standard curve of No. 16, which could be referred to Fig. 5e.

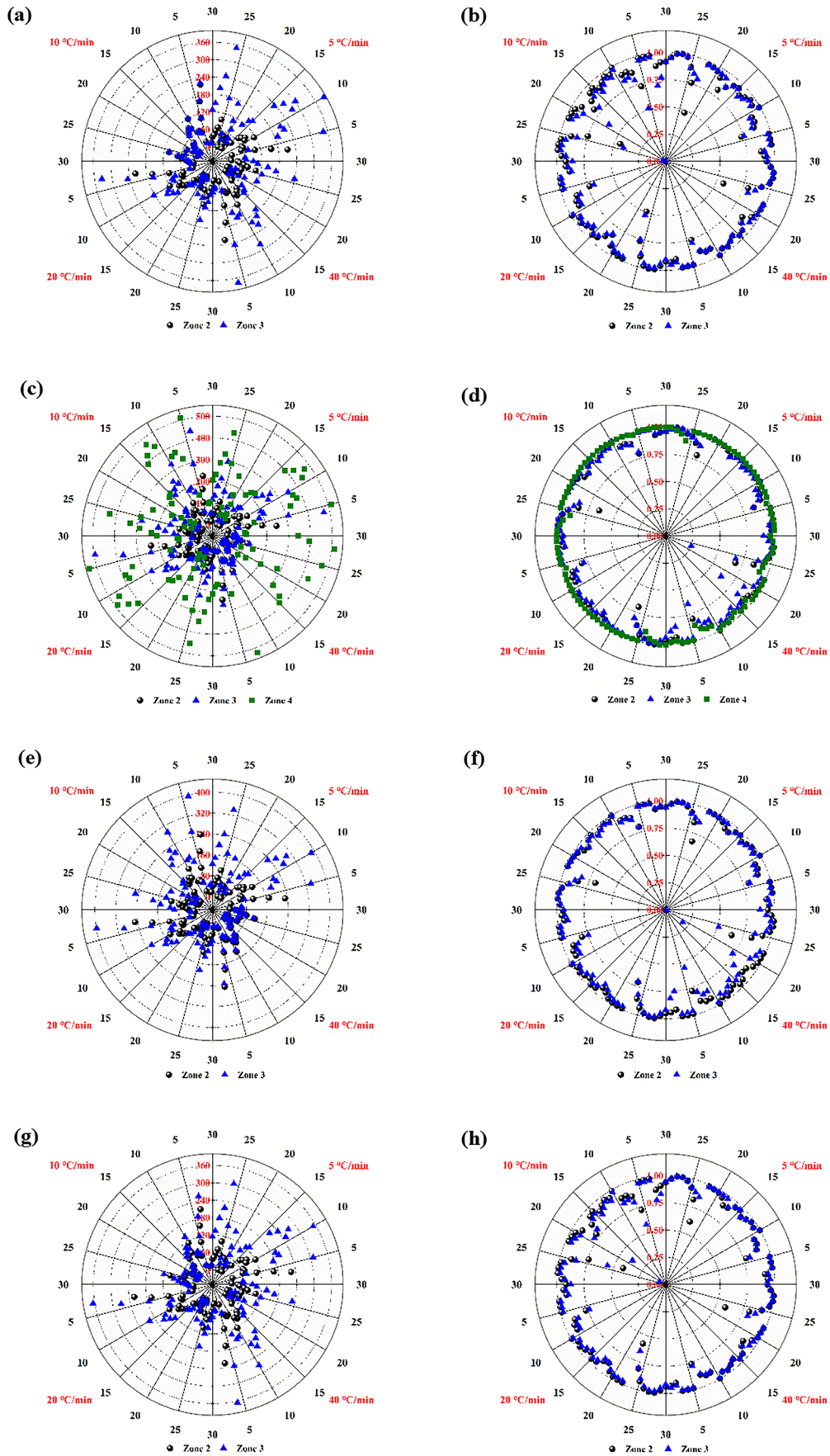


Fig. 4 Kinetic parameters of main combustion zones (Four sectors for four β s, No. 1–30 for kinetic models) E and R^2 values of **a, b** CS+10%SA, **c, d** CS+10%CaO, **e, f** CS+10%Fe₂O₃, **g, h** CS+10%SiO₂

3.6 Catalytic combustion reaction mechanisms

The catalytic combustion of solid fuels is very complicated and involves of various chemical reactions. These reactions can be characterized as dehydration reaction, chemical bonds cracking, free radical generation and recombination, gas–gas reactions between volatile matters and oxygen, gas–solid reactions between additive and depolymerizing product, and gas–solid reactions between char and oxygen, and solid–solid reactions between char and additive. The related reactions during the programmed heating process were described in Fig. 6, it specifically included:

- (1) According to the DTG curves in Fig. 3, it could be observed that there existed an obvious weight loss peak as the temperature was below about 180.0 °C, which was related to the release of various forms of moisture, such as the interstitial water, bound water, surface adsorbed water, and internal water. The process was relatively simple, which was not specified in Fig. 6.
- (2) It is well known that the biomass sample generally consists of the hemicellulose, cellulose, and lignin. As reported by Yang et al. [49], the thermal degradation of hemicellulose, cellulose, and lignin occurred at 220–315 °C, 315–400 °C, and 160–900°C, respectively. Therefore, as the reaction temperature was beyond 180.0 °C, the organics in the CS began to decompose. At around 240.0 °C, a shoulder peak could be found in the DTG curve in Fig. 2, which was due to the depolymerizing reactions of hemicellulose. The main weight loss peak was at around 280.0 °C for the cracking of

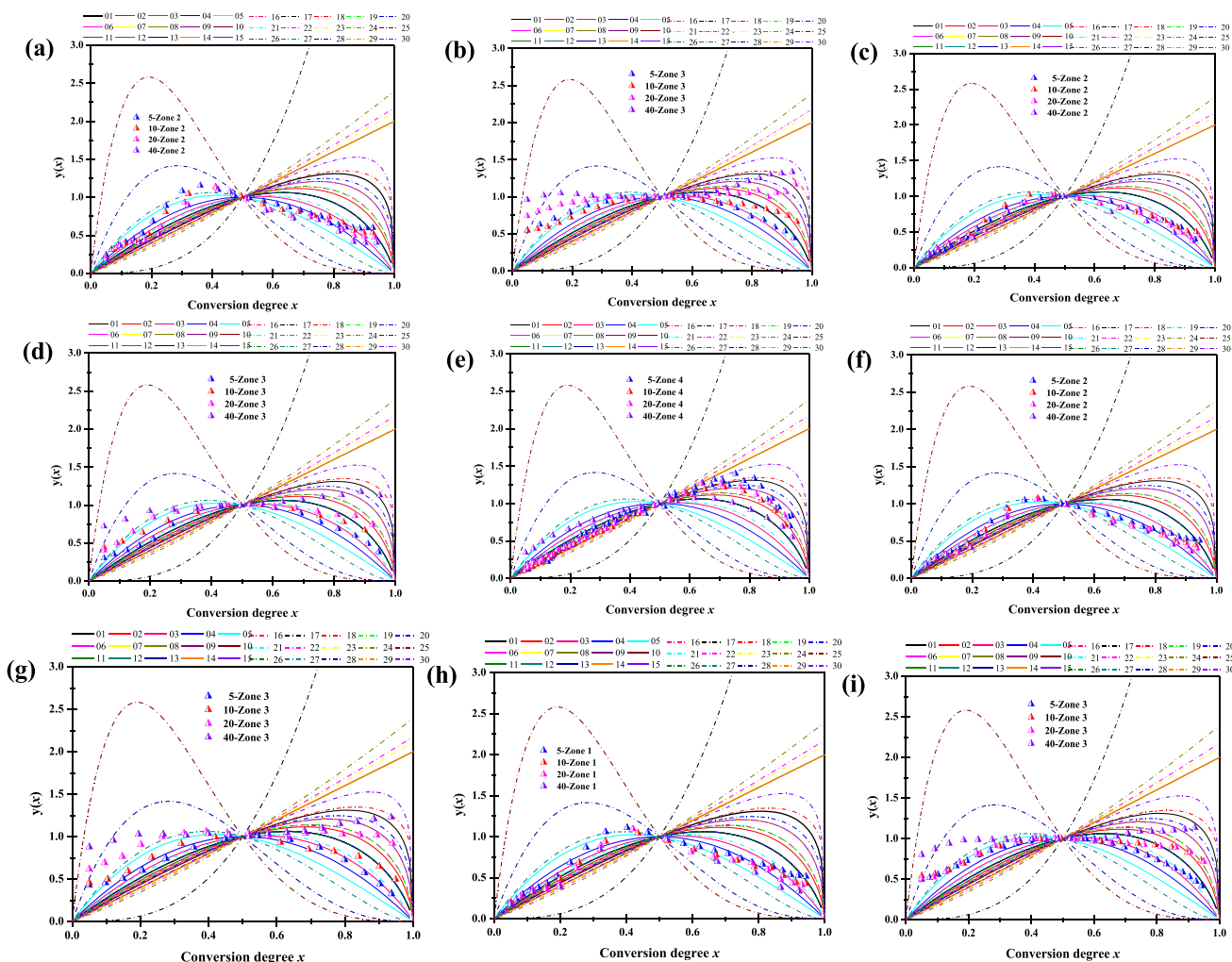


Fig. 5 Comparisons between experimental $y(x)$ from the data obtained at different β s and theoretical $y(x)$. **a, b** zone 2 and 3 of CS+10%SA, **c, d, e** zone 2, 3, and 4 of CS+10%CaO, **e, f** zone 2 and 3 of CS+10%Fe₂O₃, **g, h** zone 2 and 3 of CS+10%SiO₂

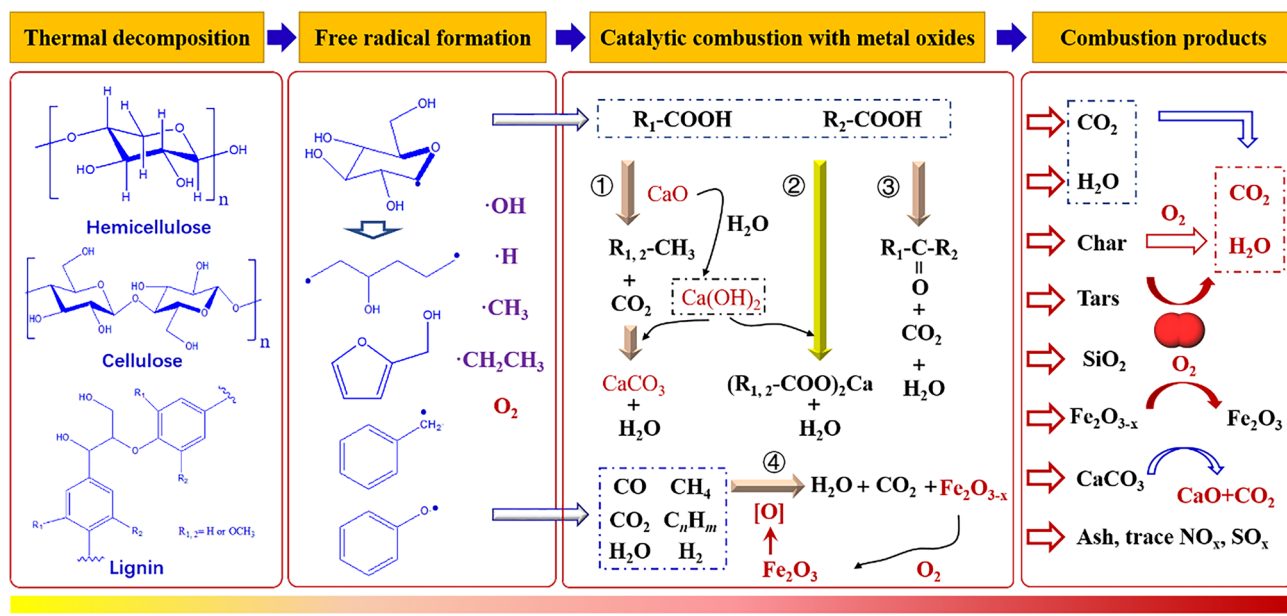


Fig. 6 The possible catalytic combustion mechanism of CS with the additions of SA and its active species of CaO , Fe_2O_3 , and SiO_2

cellulose and lignin. During the process of depolymerizing, free radicals started to be generated, and those from the cellulose and lignin could be referred to the researches of Zhang et al. [50] and Huang et al. [51], respectively. Meanwhile, the thermal degradation products of chars, tars, and non-condensable gas would be generated through the combination of free radicals. Under air atmosphere, the thermal degradation products of CS would be oxidized by oxygen, thus forming various oxygen-containing functional groups, such as C–O, –COOH, C=O, O–H, and etc.

- (3) With the additions of SA and its active species of CaO , Fe_2O_3 , and SiO_2 in this paper, the combustion process of CS would be affected. Since the existence of oxygen during the heating, the carboxylic acids ($R-COOH$) would be generated, which might be combined on the surface of CaO and SiO_2 . As a kind of alkaline oxides, CaO could act as the in-situ adsorbents of CO_2 at relatively low temperature, through the direct carbonation reaction to form $CaCO_3$ and hydrocarbons. On the other hand, CaO can be combined with the H_2O to form $Ca(OH)_2$, and then absorb CO_2 to produce $CaCO_3$. Then, by the acid–base neutralization reaction, the carboxylic acid can react with $Ca(OH)_2$ to form organic calcium salts $[(R_{1,2}-COO)_2Ca]$ and H_2O . During the combustion of $CS + 10\% SiO_2$, several sites will be provided on surface of SiO_2 , which can combine with $R-COOH$ and act as the acid catalyst, and then form the ketones, CO_2 , and H_2O . For the combustion of $CS + 10\% Fe_2O_3$, the phenomena in providing lattice oxygen $[O]$ were observed, corresponding reac-

tion paths were also described in Fig. 6. By the close contacts between Fe_2O_3 and biomass or biomass char, the transfer resistance of oxygen to carbon surface was reduced to some extent, and then effectively enhanced combustion performance of biomass. The $[O]$ transfer from metal oxides was also summarized by Zhang et al. [22] in the catalytic combustion of bituminous coal.

- (4) For the combustion products of CS with additives, with an excess air, the C and H would be respectively converted into CO_2 and H_2O , N and S might be oxidized into trace NO_x and SO_x , and the inorganics became the ash product, the additives would be regenerated by the carbonate decomposition ($CaCO_3 \rightarrow CaO + CO_2$), and lattice oxygen $[O]$ recovery ($Fe_2O_{3-x} + O_2 \rightarrow Fe_2O_3$), respectively.
- (5) From the perspective of kinetic model to understand the catalytic combustion mechanism, the kinetic models of catalytic combustion of volatiles in this research were $(1-x)^2$, i.e., unreacted core shrinkage model, which assumed that air just reacted on the surface of the unreacted nucleus, did not penetrate into the inner of core, and the reactions started from the outer surface of spherical particles. With the combustion proceeding, the surface of reactions moves to particle interior, and causes the reacted part to form a layer of ash, then the unreacted core gradually contracts inward. With regard to the catalytic combustion of chars, the kinetic functions were mainly based on the diffusion mechanism, which meant that the reactions were controlled by the air diffusion from the surface of the particles to their inner. For the zone 4 of $CS + 10\% CaO$ combustion at

varied heating rates, the kinetic models were based on shrinking core model $f(x) = 3(1-x)^{2/3}$, which is established on the assumption that the whole reactions proceed layer by layer from the surface to inner, that is to say the unreacted solid core continuously shrinks as the reaction goes on.

4 Conclusions

The effects of sludge ash (SA) and its active species of CaO, Fe₂O₃, and SiO₂ on the combustion of camellia seed shells (CS) were studied by TG-DSC. The combustion paths of CS with additions of SA, CaO, Fe₂O₃, and SiO₂ were verified. The higher heating rate signally increased combustion performance, and the CaO addition decreased combustion performance parameters. The additions of SA active species brought beneficial effects in the perspective of heat release effect. The kinetic analysis results indicated that the most of $g(x)$ kinetic functions applied all showed good linearity, which could be screened by further combining the Malek method.

Author contribution Xingui Mo: investigation, writing and draft preparation;

Jianqiang Ren: investigation, and data analysis;

Yaoyu Zhou: original draft preparation, and data analysis;

Wenhao Jiang: writing, software, and data analysis;

Jianbiao Chen: conceptualization, writing, editing, funding acquisition, supervision;

Jinjiao Zhu: data analysis, software, and editing;

Chao Wu: original draft preparation, and revision;

Yuezhao Zhu: supervision.

Funding Financial supports for this work that have been provided by the Natural Science Foundation of the Jiangsu Higher Education Institutions of China (21KJB470004).

Data availability All required/mentioned data are available in the manuscript.

Declarations

Ethical approval Not applicable.

Competing interests The authors declare no competing interests.

References

- Siddiqi H, Mishra A, Maiti P, Behera ID, Meikap BC (2022) In-situ and ex-situ co-pyrolysis studies of waste biomass with spent motor oil: elucidating the role of physical inhibition and mixing ratio to enhance fuel quality. *Bioresour Technol* 358:127364
- Siddiqi H, Bal M, Kumari U, Meikap BC (2020) In-depth physiochemical characterization and detailed thermo-kinetic study of biomass wastes to analyze its energy potential. *Renew Energy* 148:756–771
- Mishra A, Siddiqi H, Kumari U, Behera ID, Mukherjee S, Meikap BC (2021) Pyrolysis of waste lubricating oil/waste motor oil to generate high-grade fuel oil: a comprehensive review. *Renew Sustain Energy Rev* 150:111446
- Siddiqi H, Mishra A, Kumari U, Maiti P, Meikap BC (2021) Utilizing agricultural residue for the cleaner biofuel production and simultaneous air pollution mitigation due to stubble burning: a net energy balance and total emission assessment. *ACS Sustain Chem Eng* 9:15963–15972
- Ong HC, Chen WH, Singh Y, Gan YY, Chen CY, Show PL (2020) A state-of-the-art review on thermochemical conversion of biomass for biofuel production: a TG-FTIR approach. *Energy Convers Manag* 209:112634
- Sharma A, Pareek V, Zhang D (2015) Biomass pyrolysis—a review of modelling, process parameters and catalytic studies. *Renew Sustain Energy Rev* 47(9):1081–1096
- Neha S, Remya N (2023) Optimization of biochar production from microwave co-pyrolysis of food waste and low-density polyethylene. *Biomass Convers Bioresour*. <https://doi.org/10.1007/s13399-023-03948-w>
- Mu L, Li T, Wang Z, Shang Y, Yin H (2021) Influence of water/acid washing pretreatment of aquatic biomass on ash transformation and slagging behavior during co-firing with bituminous coal. *Energy* 234:121286
- Adanez J, Abad A, Garcia-Labiano F, Gayan P, Diego LF (2012) Progress in chemical-looping combustion and reforming technologies. *Prog Energy Combust* 38(2):215–282
- Gao N, Sipra AT, Quan C (2020) Thermogravimetric analysis and pyrolysis product characterization of municipal solid waste using sludge fly ash as additive. *Fuel* 281:118572
- Gao N, Milandile MH, Sipra AT, Su S, Miskolczi N, Quan C (2022) Co-pyrolysis of municipal solid waste (MSW) and biomass with Co/sludge fly ash catalyst. *Fuel* 322:124127
- Wu X, Liu J, Wei Z, Chen Z, Evrendilek F, Huang W (2022) Oxy-fuel co-combustion dynamics of phytoremediation biomass and textile dyeing sludge: gas-to-ash pollution abatement. *Sci Total Environ* 825:153656
- Huang H, Liu J, Evrendilek F, Zhang G, Sun S, He Y (2022) Bottom slag-to-flue gas controls on S and Cl from co-combustion of textile dyeing sludge and waste biochar: their interactions with temperature, atmosphere, and blend ratio. *J Hazard Mater* 435:129007
- Hu J, Song Y, Liu J, Evrendilek F, Zhang G, Ren M, Xie W, Sun S (2022) Torrefaction-assisted oxy-fuel co-combustion of textile dyeing sludge and bamboo residues toward enhancing emission-to-ash desulfurization in full waste circularity. *Fuel* 318:123603
- Idris SS, Rahman NA, Ismail K (2012) Combustion characteristics of Malaysian oil palm biomass, sub-bituminous coal and their respective blends via thermogravimetric analysis (TGA). *Bioresour Technol* 123:581–591
- Chen J, Wang Y, Lang X, Ren X, Fan S (2017) Comparative evaluation of thermal oxidative decomposition for oil-plant residues via thermogravimetric analysis: thermal conversion characteristics, kinetics, and thermodynamics. *Bioresour Technol* 243:37–46
- Wang SJ, Wu F, Zhang G, Zhu P, Wang ZY, Huang CJ, Chen ST (2014) Research on the combustion characteristics of anthracite and blended coal with composite catalysts. *J Energy Inst* 87:96–101
- Liu Z, Wang G, Li P, Li C (2019) Investigation on combustion of high-sulfur coal catalyzed with industrial waste slags. *J Energy Inst* 92:621–629
- Xu F, Xing X, Gao S, Zhang W, Zhu L, Wang Y, Chen J, Chen H, Zhu Y (2021) Direct chemical looping gasification of pine sawdust using Fe₂O₃-rich sludge ash as an oxygen carrier: thermal conversion characteristics, product distributions, and gasification performances. *Fuel* 304:121499

20. Zou C, Zhao J (2017) Investigation of iron-containing powder on coal combustion behavior. *J Energy Inst* 90:797–805
21. Gong Z, Wu W, Zhao Z, Li B (2018) Combination of catalytic combustion and catalytic denitration on semi-coke with Fe₂O₃ and CeO₂. *Catal Today* 318:59–65
22. Zhang H, Dou B, Li J, Zhao L, Wu K (2020) Thermogravimetric kinetics on catalytic combustion of bituminous coal. *J Energy Inst* 93:2526–2535
23. Cai J, Wang S, Kuang C, Tang X (2017) Insight into the kinetic analysis of catalytic combustion for biomass after alkaline metals loaded pretreatment. *Fuel* 203:501–513
24. Cheng J, Zhou F, Xuan X, Liu J, Zhou J, Cen K (2017) Comparison of the catalytic effects of eight industrial wastes rich in Na, Fe, Ca and Al on anthracite coal combustion. *Fuel* 187(1):398–402
25. Song Y, Hu J, Liu J, Evrendilek F, Buyukada M (2020) Catalytic effects of CaO, Al₂O₃, Fe₂O₃, and red mud on *Pteris vittata* combustion: emission, kinetic and ash conversion patterns. *J Clean Prod* 252:119646
26. Hu J, Yan Y, Song Y, Liu J, Evrendilek F, Buyukada M (2020) Catalytic combustions of two bamboo residues with sludge ash, CaO, and Fe₂O₃: bioenergy, emission and ash deposition improvements. *J Clean Prod* 270:122418
27. Huang Z, Deng Z, Chen D, He F, Liu S, Zhao K, Wei G, Zheng A, Zhao Z, Li H (2017) Thermodynamic analysis and kinetic investigations on biomass char chemical looping gasification using Fe–Ni bimetallic oxygen carrier. *Energy* 141:1836–1844
28. Yan X, Hu J, Zhang Q, Zhao S, Dang J, Wang W (2020) Chemical-looping gasification of corn straw with Fe-based oxygen carrier: thermogravimetric analysis. *Bioresour Technol* 303:122904
29. Xu X, Li Z, Jiang E (2019) Torrefaction performance of camellia shell under pyrolysis gas atmosphere. *Bioresour Technol* 284:178–187
30. Zhang C, Li S, Ouyang S, Tsang CW, Xiong D, Yang K, Zhou Y, Xiao Y (2021) Co-pyrolysis characteristics of camellia oleifera shell and coal in a TGA and a fixed-bed reactor. *J Anal Appl Pyrol* 155:105035
31. Deng T, Yu Z, Zhang X, Zhang Y, Chen L, Ma X (2020) Catalytic co-pyrolysis behaviors and kinetics of camellia shell and take-out solid waste using pyrolyzer - gas chromatography/mass spectrometry and thermogravimetric analyzer. *Bioresour Technol* 297:122419
32. Meng F, Yu J, Tahmasebi A, Han Y (2013) Pyrolysis and combustion behavior of coal gangue in O₂/CO₂ and O₂/N₂ mixtures using thermogravimetric analysis and a drop tube furnace. *Energy Fuels* 27:2923–2932
33. Gai C, Dong Y, Zhang T (2013) The kinetic analysis of the pyrolysis of agricultural residue under non-isothermal conditions. *Bioresour Technol* 127:298–305
34. Mishra RK, Mohanty K (2018) Pyrolysis kinetics and thermal behavior of waste sawdust biomass using thermogravimetric analysis. *Bioresour Technol* 251:63–74
35. Mu L, Wang R, Zhai Z, Zhang B, Shang Y, Yin H (2021) Evaluation of thermokinetics methodology, parameters, and coke characterization of co-pyrolysis of bituminous coal with herbaceous and agricultural biomass. *Biomass Convers Bioresour*. <https://doi.org/10.1007/s13399-021-01502-0>
36. Siddiqi H, Biswas S, Kumari U, Bindu VNVH, Mukherjee S, Meikap BC (2021) A comprehensive insight into devolatilization thermo-kinetics for an agricultural residue: towards a cleaner and sustainable energy. *J Clean Prod* 310:127365
37. Siddiqi H, Kumari U, Biswas S, Mishra A, Meikap BC (2020) A synergistic study of reaction kinetics and heat transfer with multi-component modelling approach for the pyrolysis of biomass waste. *Energy* 204:117933
38. Chen B, Yao Z, Zhang C, Cheng S, Zhu M, Wang Y, Wu Y, Cao H, Watson I, Cai D (2023) Catalytic co-pyrolysis of cellulosic ethanol-processing residue with high-density polyethylene over biomass bottom ash catalyst. *Biomass Convers Bioresour*. <https://doi.org/10.1007/s13399-023-03915-5>
39. Vlaev L, Nedelchev N, Gyurova K, Zagorcheva M (2008) A comparative study of non-isothermal kinetics of decomposition of calcium oxalate monohydrate. *J Anal Appl Pyrol* 81:253–262
40. Singh RK, Patil T, Sawarkar AN (2020) Pyrolysis of garlic husk biomass: physico-chemical characterization, thermodynamic and kinetic analyses. *Bioresour Technol Rep* 12:100558
41. Luo L, Zhang Z, Li C, Shu N, He F, Zhang X, Cai J (2021) Insight into master plots method for kinetic analysis of lignocellulosic biomass pyrolysis. *Energy* 233:121194
42. Malek J (1992) The kinetic analysis of nonisothermal data. *Thermochim Acta* 200:257–269
43. Chen J, Xu W, Zhu L, Xu F, Mu L, Wang Y, Zhu Y (2021) Thermal conversion behaviors, kinetics, and thermodynamics of wastewater sludge via thermogravimetric analysis, and emission characteristics from a large-scale incinerator. *J Mater Cycles Waste* 23:1466–1478
44. Xie Z, Ma X (2013) The thermal behaviour of the co-combustion between paper sludge and rice straw. *Bioresour Technol* 146:611–618
45. Li J, Dou B, Zhang H, Zhang H, Chen H, Xu Y (2021) Thermochemical characteristics and non-isothermal kinetics of camphor biomass waste. *J Environ Chem Eng* 9:105311
46. Song Y, Liu J, Evrendilek F, Kuo J, Buyukada M (2019) Combustion behaviors of *Pteris vittata* using thermogravimetric, kinetic, emission and optimization analyses. *J Clean Prod* 237:117772
47. Fang S, Yu Z, Lin Y, Lin Y, Fan Y, Liao Y, Ma X (2016) Effects of additives on the co-pyrolysis of municipal solid waste and paper sludge by using thermogravimetric analysis. *Bioresour Technol* 209:265–272
48. Fang S, Yu Z, Lin Y, Lin Y, Fan Y, Liao Y, Ma X (2017) A study on experimental characteristic of co-pyrolysis of municipal solid waste and paper mill sludge with additives. *Appl Therm Eng* 111:292–300
49. Yang H, Yan R, Chen H, Lee DH, Zheng C (2007) Characteristics of hemicellulose, cellulose and lignin pyrolysis. *Fuel* 86:1781–1788
50. Zhang X, Li J, Yang W, Blasiak W (2011) Formation mechanism of levoglucosan and formaldehyde during cellulose pyrolysis. *Energy Fuel* 25(8):3739–3746
51. Huang S, Qin J, Chen T, Yi C, Zhang S, Zhou Z, Zhou N (2022) Co-pyrolysis of different torrefied Chinese herb residues and low-density polyethylene: kinetic and products distribution. *Sci Total Environ* 802:149752

Publisher's note Springer Nature remains neutral with regard to jurisdictional claims in published maps and institutional affiliations.

Springer Nature or its licensor (e.g. a society or other partner) holds exclusive rights to this article under a publishing agreement with the author(s) or other rightsholder(s); author self-archiving of the accepted manuscript version of this article is solely governed by the terms of such publishing agreement and applicable law.